Structural Engineering and Mechanics, *Vol. 66, No. 5 (2018) 595-608*
DOI: https://doi.org/10.12989/sem.2018.66.5.595

Dynamic behavior of footbridges strengthened by external cable systems

Ioannis G. Raftoyiannis* and George T. Michaltsos[a]

Department of Civil Engineering, National Technical University of Athens, 9 Iroon Polytechneiou Str., Athens 15780, Greece

(Received October 12, 2016, Revised February 9, 2018, Accepted February 12, 2018)

Abstract. This paper deals with the lateral - torsional motion of bridges provided with external cables acting as dampers under the action of horizontal dynamic loads or of walking human crowd loads. A three dimensional analysis is performed for the solution of the bridge models. The theoretical formulation is based on a continuum approach, which has been widely used in the literature to analyze bridges. The resulting equations of the uncoupled motion are solved using the Laplace Transformation, while the case of the coupled motion is solved through the use of the potential energy. Finally, characteristic examples are presented and useful results are obtained

Keywords: bridges; stay cables; footbridges; dynamic behaviour; damping systems

1. Introduction

Footbridges are a useful special type of bridges, which due to their particular form, their geometrical characteristics as well as their relatively small live loads, are very often badly designed and secondary dynamic phenomena are neglected. The most frequently appeared problems are those of lateral and torsional (coupled or uncoupled) vibrations due to human crowd loadings, especially from pedestrians in marching.

There are numerous works studying the vertical and lateral motion of such bridges by analytical or experimental way such as the ones by Bachman and Ammann (1987), Fujino *et al.* (1992, 1993), Stoyanoff (1992), and others.

On June 2000, the Millennium footbridge in London, which has been built across the river Thames, has opened for the public. In the opening ceremony, a crowd of over 1000 people had assembled on the south half of the bridge with a band in front. When the crowd started to walk across with the band playing, there was immediately an unexpectedly pronounced lateral movement of the bridge deck. This movement became sufficiently large for people to stop walking in order to retain their balance and sometimes to hold onto the handrails for support. Video pictures showed later that the south span had been moving with amplitude of about 50 mm at 0.8 Hz and the central span about 75 mm at 1 Hz, approximately.

It was decided immediately to limit the number of people on the bridge, but even so the deck movement was sufficient to be uncomfortable and to raise concern for public safety so that on June 12, 2000, the bridge was closed in order to find a solution for the problem. The footbridge remained closed and has reopened for the public on February 22, 2002.

Fig. 1 The London Millennium footbridge shortly after its completion

It was realized very quickly that the problem was due to lateral excitation. Therefore, it became necessary to strengthen the bridge. Thus, strengthening of the bridge with external cables was chosen as a solution. As a result, the set cables carry a very high tensile force for a bridge of this size, totaling about 2000 tons-see Fig. 1.

A significant number of publications followed by, where the case of strengthening of a bridge with external cables has been investigated. External cables are usually employed to cope with unexpectedly large lateral or torsional deformations in existing bridges. These phenomena are usually appearing due to incorrect or improper design. On this field, one must refer to the studies of Dallard *et al.* (2001), Nakamura and Kawasaki (2006), Eckhard and Ott (2006), Roberts *et al.* (2006), Ingolfsson and Georgakis (2011), Ingolfsson *et al.* (2012), Li *et al.* (2013), Lonetti and Pascuzzo (2014), Racic and Morin (2014), Zhang and Yu (2015), Zhang and Zhang (2016) and Sun *et al.* (2016).

*Corresponding author, Associate Professor
E-mail: rafto@central.ntua.gr
[a]Professor
E-mail: michalts@central.ntua.gr

http://www.techno-press.com/journals/sem&subpage=7
ISSN: 1225-4568 (Print), 1598-6217 (Online)

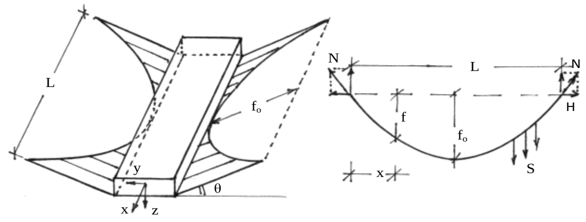

(a) (b)

Fig. 2(a) Perspective, and (b) side-view of a cable-damper

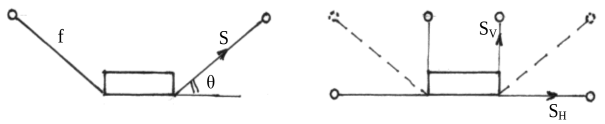

(a) (b)

Fig. 3(a) Cable system, and (b) equivalent vertical and horizontal systems

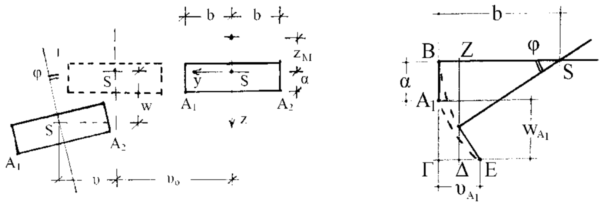

(a) (b)

Fig. 4(a) displacements of the deck, and (b) detailed analysis

The present paper deals with the lateral-torsional motion of a bridge provided with external cables as dampers under the action of horizontal dynamic loads or of walking human crowd loads. A 3-D analysis is performed for the solution of the bridge models. The theoretical formulation is based on a continuum approach, which has been widely used in the literature to analyze bridges. The resulting equations of the uncoupled motion are solved using the Laplace Transformation, while the case of the coupled motion is solved through the use of the potential energy. The method presented herein has been verified via the FE method as well as the exact solution of lateral-torsional motion of beams, the basics of which are given in the Appendix.

Finally, characteristic examples are presented and useful results are obtained.

2. Basic assumptions

1. A damping system, consisted of cables such as the ones shown in Fig. 2, is applied on an inclined plane by angle θ.

2. The initial stretching of the hangers is S_o, while under dynamic loading it becomes $S = S_o + S_e$

3. An arbitrary point of the bridge at x (Fig. 2), under the action of an earthquake motion governed by $\upsilon_o(t)$, is displaced as shown in Fig. 3.

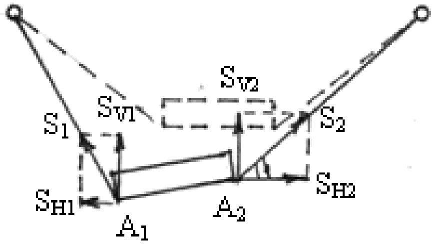

(a)

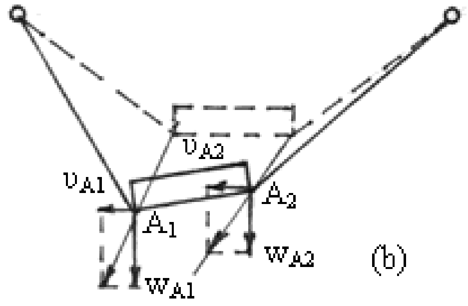

(b)

Fig. 5(a) Forces, and (b) displacements of the deck

4. It is also considered that: $f\left(\frac{L}{2}\right) = f_o$

5. Under the action of dead and vertical live loads, it is $\upsilon = 0$, w=0, φ=0 and $S = S_o$.

3. Introductory concepts

1. The system studied is shown in Fig. 2(a). The external cables have length L, sag f_o and are set inclined by angle θ. For the initial stress N, we have the horizontal component H and stresses S of the hangers.

2. The above system is analyzed into the systems of Fig. 3(b), consisting of one vertical with sag f_V, f_{Vo} and stress of the hangers S_V and one horizontal with f_H, f_{Ho} and S_H, respectively.

The following relations are valid

$$\left.\begin{aligned} S_V &= S \cdot \sin\theta \quad f_{Vo} = f_o \sin\theta \\ S_H &= S \cdot \cos\theta \quad f_{Ho} = f_o \cos\theta \end{aligned}\right\} \tag{1}$$

According to the theory of cables, their tensions will be

$$\left.\begin{aligned} H_V &= \frac{S_V L^2}{8 f_{Vo}} = \frac{S \cdot \sin\theta \cdot L^2}{8 f_o \sin\theta} = \frac{S \cdot L^2}{8 \cdot f_o} = H \\ H_H &= \frac{S_H L^2}{8 f_{Ho}} = \frac{S \cdot \cos\theta \cdot L^2}{8 f_o \cos\theta} = \frac{S \cdot L^2}{8 \cdot f_o} = H \end{aligned}\right\} \tag{2}$$

3. The following relations are valid

$$\left.\begin{aligned} &H = H_o + H_e\,, \quad S = -H \cdot (f + \Delta f)''\,, \quad H_e = -\frac{f''}{L_c / E_c F_c} \cdot \int_0^L \Delta f \, dx \\ &f(x) = \frac{4 f_o}{L^2}(Lx - x^2), \quad L_c = L\left(1 + \frac{8 f_o^2}{L^2}\right) \;, \quad H_o = \frac{S_o L^2}{8 f_o}, \quad H_o = -\frac{g}{f''} \end{aligned}\right\} \tag{3}$$

4. The deck

Separating the deck and showing its motion because of the action of a horizontal load, we get Fig. 4(a), showing the displacement of a cross-section of the deck, where υ_o is the ground motion and $\upsilon, w,$ and φ are the displacements and the angle of rotation of the cross-section's gravity center.

Because of the angle φ, the points A_1 and A_2 have additional displacements determined as follows, taking into account that φ<10^o and so $\cos\varphi \cong 1$, $\sin\varphi \cong \varphi$. The following relations are valid (see also Fig. 4(b))

$$\left.\begin{aligned}&\overline{BZ} = \overline{Z\Delta} = \overline{ZB'} + \overline{B'\Delta} = b\sin\varphi + \alpha\cos\varphi \cong b\varphi + \alpha\\&dw = \overline{\Gamma A_1} = \overline{B\Gamma} - \alpha \cong b\varphi + \alpha - \alpha = b\varphi\\&d\upsilon = \overline{\Gamma E} = \overline{\Gamma\Delta} + \overline{\Delta E} = \overline{BZ} + \overline{\Delta E} = \overline{BS} - \overline{ZS} + \overline{\Delta E} = b - b\cos\varphi + \alpha\sin\varphi \cong \alpha\varphi\end{aligned}\right\}$$

Therefore, the displacements of points A_1 and A_2 are

$$\left.\begin{aligned}A_1:\ &\text{parallel to } S_y:\ \upsilon_{A1} = \upsilon - \alpha\varphi\\&\quad"\quad"\quad S_z:\ w_{A1} = w + b\varphi\\A_2:\ &\quad"\quad"\quad S_y:\ \upsilon_{A2} = \upsilon + \alpha\varphi\\&\quad"\quad"\quad S_z:\ w_{A2} = W - b\varphi\end{aligned}\right\} \tag{4}$$

5. The acting forces

In Fig. 5(b), one can see the displacements of the points A_1 and A_2 (where they are joined the hangers), because of live or dynamic loadings.

One can observe that applying the positive signs for υ, w and φ some displacements cause additional strain on hangers, while the rest cause looseness of hangers (see Fig. 5b). This remark is taken into account in the following analysis.

5.1 The vertical forces

Marking by the index "o" the forces without dynamic loadings and by "e" the additional forces because of dynamic loads we have

$$\left.\begin{aligned}P_z &= g + p_z(x,t) - c_z\dot{w} - m\ddot{w} - (S_{V1} + S_{V2}) =\\&= g + p_z(x,t) - c_z\dot{w} - m\ddot{w} + (H_{V1} + H_{Ve1})(f_V + w_1)'' + (H_{V2} + H_{Ve2})(f_V + w_2)'' =\\&= g + p_z(x,t) - c_z\dot{w} - m\ddot{w} + 2H_o f_V'' + H_o(w_1'' + w_2'') + H_{Ve1}f_V'' + H_{Ve2}f_V''\end{aligned}\right\}$$

or finally

$$\left.\begin{aligned}&P_z = p_z(x,t) - c_z\dot{w} - m\ddot{w} + 2H_o w'' - \frac{2f_V''^2}{L_{cV}/E_cF_c}\cdot\int_0^L w dx\\&\text{with: } f_V'' = -\frac{8f_o}{L^2}\cdot\sin\theta, \quad\text{and}\quad L_{cV} = \left(1 + \frac{8f_o^2\cdot\sin^2\theta}{L^2}\right)\end{aligned}\right\} \tag{5}$$

where Eqs. (3), and (4) are taken into account and also that $\Delta f << f$.

5.2 The horizontal forces

Following a similar procedure with §5.1 we have

$$\begin{aligned}P_y &= p_y(x,t) - c_z(\dot{\upsilon} + \dot{\upsilon}_o) - m(\ddot{\upsilon} + \ddot{\upsilon}_o) + S_{H1} - S_{H2} =\\&= p_y(x,t) - c_z(\dot{\upsilon} + \dot{\upsilon}_o) - m(\ddot{\upsilon} + \ddot{\upsilon}_o)\\&-(H_{H1} - H_{He1})(f_H - \upsilon_1)'' + (H_{H2} + H_{He2})(f_H + \upsilon_2)''\end{aligned}$$

Because of Eqs. (3) and (4), we finally obtain

$$\left.\begin{aligned}&P_y = p_y(x,t) - c_z(\dot{\upsilon} + \dot{\upsilon}_o) - m(\ddot{\upsilon} + \ddot{\upsilon}_o) + 2H_o\upsilon'' - \frac{2f_H''^2}{L_{cH}/E_cF_c}\cdot\int_0^L \upsilon dx\\&\text{with: } f_H'' = -\frac{8f_o}{L^2}\cdot\cos\theta, \quad\text{and}\quad L_{cH} = \left(1 + \frac{8f_o^2\cdot\cos^2\theta}{L^2}\right)\end{aligned}\right\} \tag{6}$$

where $\upsilon_o(t)$ is the soil motion, while it is taken into account that a positive υ_{A1} brings about looseness of the cable 1.

5.3 The torsional moments

Taking into account §5.1 and 5.2 we obtain

$$M_x = m_x(x,t) - c_\varphi\dot{\varphi} - J_{px}\ddot{\varphi} - S_{V1}b + S_{V2}b - S_{H1}(\alpha + z_M) + S_{H2}(\alpha + z_M)$$

or finally

$$\left.\begin{aligned}&M_x = m_x(x,t) - c_\varphi\dot{\varphi} - J_{px}\ddot{\varphi} - \frac{2b^2\cdot f_V''^2}{L_{cV}/E_cF_c}\int_0^L \varphi dx +\\&+ \frac{2(z_M + \alpha)f_H''^2}{L_{cH}/E_cF_c}\int_0^L \upsilon dx\end{aligned}\right\} \tag{7}$$

6. The equations of motion

Taking into account Eqs. (5), (6), (7) and that the external loadings can be expressed as relations of t, the complete equations of motion are given by the following expressions

$$\left.\begin{aligned}&EI_y w'''' - 2H_o w'' + c_y\dot{w} + m\ddot{w} = p_z(x,t) + B_V\int_0^L w dx\\&EI_z(\upsilon + \upsilon_o)'''' - EI_z\cdot z_M\varphi'''' - 2H_o\upsilon'' + c_z(\dot{\upsilon} + \dot{\upsilon}_o) + m(\ddot{\upsilon} + \ddot{\upsilon}_o) =\\&\qquad = p_y(x,t) - B_H\int_0^L \upsilon dx\\&EI_\omega\varphi'''' - EI_z\cdot z_M(\upsilon + \upsilon_o)'''' - GI_d\varphi'' + c_\varphi\dot{\varphi} + I_{px}\ddot{\varphi} =\\&\qquad = m_t(x,t) - b^2\cdot B_V\int_0^L \varphi dx + (z_M + \alpha)B_H\int_0^L \upsilon dx\\&\text{with:}\quad B_V = \frac{2f_V''^2}{L_{cV}/E_cF_c},\quad B_H = \frac{2f_H''^2}{L_{cH}/E_cF_c}\\&\text{and:}\quad p_y(x,t) = p_y(x)\cdot f_y(t),\quad p_z(x,t) = p_z(x)\cdot f_z(t),\\&\qquad m_x(x,t) = m_x(x)\cdot f_x(t)\end{aligned}\right\} \tag{8}$$

7. Doubly symmetric cross-section

For a bridge, the deck of which has a doubly symmetric cross-section, it will be $z_M = 0$, α=0, and therefore Eq. (8) become uncoupled

$$\left.\begin{aligned}&EI_y w'''' - 2H_o w'' + c_y\dot{w} + m\ddot{w} = p_z(x,t) - B_V\int_0^L w dx\\&EI_z\upsilon'''' - 2H_o\upsilon'' + c_z\dot{\upsilon} + m\ddot{\upsilon} = p_y(x,t) - EI_z\dot{\upsilon}_o - c_z\dot{\upsilon}_o - m\ddot{\upsilon}_o - B_H\int_0^L \upsilon dx\\&EI_\omega\varphi'''' - GI_d\varphi'' + c_\varphi\dot{\varphi} + I_{px}\ddot{\varphi} = m_t(x,t) - b^2 B_V\int_0^L \varphi dx\end{aligned}\right\} \tag{9}$$

In this case, we observe that all equations are independent each other and therefore they can be solved separately.

7.1 The vertical motion

In order to solve Eq. (9a), we are searching for a solution of the form

$$w(x,t) = \sum_{\rho=1}^{n} W_\rho(x)\cdot T_\rho(t) \tag{10a}$$

where $T_\rho(t)$ are the time functions under determination and $W_\rho(x)$ are functions arbitrarily chosen that satisfy the boundary conditions. As such functions we choose the shape functions of a single span beam with axial force $2H_o \sin\theta$, given by Michaltsos and Raftoyiannis (2012)

$$\left.\begin{aligned} W_\rho(x) &= c_1\left(\sin\lambda_1 x - \frac{\sin\lambda_1 L}{\mathrm{Sinh}\lambda_2 L}\cdot \mathrm{Sinh}\lambda_2 x\right)\\ \text{where: }\ \lambda_1 &= \sqrt{-\frac{H_o}{EI_y}+\sqrt{\left(\frac{H_o}{EI_y}\right)^2+\frac{m\omega_{y\rho}^2}{EI_y}}}\\ \lambda_2 &= \sqrt{\frac{H_o}{EI_y}+\sqrt{\left(\frac{H_o}{EI_y}\right)^2+\frac{m\omega_{y\rho}^2}{EI_y}}} \end{aligned}\right\} \tag{10b}$$

while $\omega_{y\rho}$ are given by the relation

$$\omega_{y\rho} = \sqrt{\frac{\rho^4\pi^4 EI_y}{mL^4}+\frac{2\rho^2\pi^2 H_o}{mL^2}} \qquad \rho = 1, 2, 3, ... \tag{10c}$$

Introducing expression (10a) into Eq. (9a) we obtain

$$\left.\begin{aligned} EI_y\sum_{\rho=1}^{n} W_\rho'''' T_\rho - 2H_o\sum_{\rho=1}^{n} W_\rho'' T_\rho + c_y\sum_{\rho=1}^{n} W_\rho \dot{T}_\rho + m\sum_{\rho=1}^{n} W_\rho \ddot{T}_\rho &= \\ = p_z - B_V\int_0^L \sum_{\rho=1}^{n} W_\rho T_\rho dx & \end{aligned}\right\} \tag{11a}$$

Remembering that $W_\rho(x)$ satisfies the equation of free motion

$$EI_y W_\rho'''' - 2H_o W_\rho'' - m\omega_{y\rho}^2 W_\rho = 0 \tag{11b}$$

Eq. (11a) becomes

$$m\sum_{\rho=1}^{n} W_\rho \ddot{T}_\rho + c_y\sum_{\rho=1}^{n} W_\rho \dot{T}_\rho + m\sum_{\rho=1}^{n}\omega_{y\rho}^2 W_\rho T_\rho = p_z - B_V\int_0^L\sum_{\rho=1}^{n} W_\rho T_\rho dx \tag{11c}$$

Multiplying the above by $W_\rho(x)$ and integrating from 0 to L we get

$$\ddot{T}_\rho + \frac{c_y}{m}\dot{T}_\rho + \omega_{y\rho}^2 T_\rho = \frac{\int_0^\alpha p_z W_\rho dx}{m\int_0^L W_\rho^2 dx}\cdot f_z(t) - \frac{\int_0^L W_\rho dx}{m\int_0^L W_\rho^2 dx}\cdot B_V\int_0^L\sum_{\rho=1}^{n} W_\rho T_\rho dx \tag{11d}$$

with α from Fig. 7.

In order to solve the above system Eq. (11d), we use the Laplace Transformation with initial conditions $T_\rho(0) = \dot{T}_\rho(0) = 0$. Thus, we set

$$\left.\begin{aligned} LT_\rho(t) &= G_\rho(s)\\ Lf_z(t) &= F_z(s)\\ L\dot{T}_\rho(t) &= s\cdot G_\rho(s)\\ L\ddot{T}_\rho(t) &= s^2\cdot G_\rho(s) \end{aligned}\right\} \tag{11e}$$

Therefore, the system of Eq. (11d) becomes

$$\left.\begin{aligned} a_{\rho1}G_1 + a_{\rho2}G_2 + \cdots + a_{\rho k}G_k + \cdots a_{\rho\rho}G_\rho + \cdots a_{\rho n}G_n &= B_\rho\\ \text{where: }\ a_{\rho k} &= \frac{B_v\int_0^L W_\rho dx\int_0^L W_k dx}{m\int_0^L W_\rho^2 dx}\\ a_{\rho\rho} &= \frac{B_v\left(\int_0^L W_\rho dx\right)^2}{m\int_0^L W_\rho^2 dx} + s^2 + \frac{c_y}{m}\cdot s + \omega_{y\rho}^2\\ B_\rho &= \frac{\int_0^\alpha p_z W_\rho dx}{m\int_0^L W_\rho^2 dx}\cdot F_z(s) \end{aligned}\right\} \tag{11f}$$

and finally

$$T_\rho(t) = L^{-1}G_\rho(s) \tag{11g}$$

7.2 The lateral motion

In order to solve Eq. (9a), we are searching for a solution of the form

$$\upsilon(x,t) = \sum_{\rho=1}^{n} V_\rho(x)\cdot R_\rho(t) \tag{12a}$$

where $R_\rho(t)$ are the time functions under determination and $V_\rho(x)$ are functions arbitrarily chosen that satisfy the boundary conditions. As such functions, we choose the shape functions of a single span beam with axial force $2H_o \cos\theta$, given by Michaltsos and Raftoyiannis (2012)

$$\left.\begin{aligned} V_\rho(x) &= c_1\left(\sin\xi_1 x - \frac{\sin\xi_1 L}{\mathrm{Sinh}\xi_2 L}\cdot \mathrm{Sinh}\xi_2 x\right)\\ \text{where: }\ \xi_1 &= \sqrt{-\frac{H_o}{EI_z}+\sqrt{\left(\frac{H_o}{EI_z}\right)^2+\frac{m\omega_{z\rho}^2}{EI_z}}}\\ \xi_2 &= \sqrt{\frac{H_o}{EI_z}+\sqrt{\left(\frac{H_o}{EI_z}\right)^2+\frac{m\omega_{z\rho}^2}{EI_z}}} \end{aligned}\right\} \tag{12b}$$

while $\omega_{z\rho}$ are given by the relation

$$\omega_{z\rho} = \sqrt{\frac{\rho^4\pi^4 E I_z}{m L^4} + \frac{2\rho^2\pi^2 H_o}{m L^2}} \qquad \rho = 1, 2, 3, ... \tag{12c}$$

Introducing (12a) into (9b) and Following the procedure of §7.1 we conclude to the system

$$\left.\begin{aligned} \ddot{R}_\rho + \frac{c_z}{m}\cdot\dot{R}_\rho + \omega_{z\rho}^2 R_\rho &= \frac{f_y(t)\int_0^L p_y V_\rho dx - (c_z\dot{\upsilon}_o + m\ddot{\upsilon}_o)\int_0^L V_\rho dx}{m\int_0^L V_\rho^2 dx} - \\ &- \frac{B_H\int_0^L V_\rho dx}{m\int_0^L V_\rho^2 dx}\cdot\int_0^L\sum_{\rho=1}^n V_\rho R_\rho dx \end{aligned}\right\} \tag{12d}$$

In order to solve the above system of Eq. (12d), we use the Laplace Transformation with initial conditions $R(0) = \dot{R}(0) = 0$. We set

$$\left.\begin{aligned} &LR_\rho(t) = K_\rho(s),\quad L\dot{R}_\rho(t) = s\cdot K_\rho(s),\quad L\ddot{R}_\rho(t) = s^2\cdot K_\rho(s) \\ &Lf_z(t) = F_z(s),\quad L\upsilon_o(t) = U_o(s),\quad L\dot{\upsilon}_o(t) = s\cdot U_o(s),\quad L\ddot{\upsilon}_o(t) = s^2\cdot U_o(s) \end{aligned}\right\} \tag{12e}$$

Therefore, the system (12d) becomes

$$\left.\begin{aligned} &b_{\rho1}K_1 + b_{\rho2}K_2 + \cdots + b_{\rho k}K_k + \cdots b_{\rho\rho}K_\rho + \cdots + b_{\rho n}K_n = \Gamma_\rho \\ &\text{where:}\quad b_{\rho k} = \frac{B_H\int_0^L V_\rho dx\int_0^L V_k dx}{m\int_0^L V_\rho^2 dx} \\ &b_{\rho\rho} = \frac{B_H\left(\int_0^L V_\rho dx\right)^2}{m\int_0^L V_\rho^2 dx} + s^2 + \frac{c_z}{m}\cdot s + \omega_{z\rho}^2 \\ &\Gamma_\rho = \frac{\int_0^L p_y V_\rho dx}{m\int_0^L V_\rho^2 dx}\cdot F_z(s) - \frac{\int_0^L V_\rho dx}{m\int_0^L V_\rho^2 dx}\cdot(c_z\cdot s + m\cdot s^2)\cdot U_o(s) \end{aligned}\right\} \tag{12f}$$

and finally

$$R_\rho(t) = L^{-1}K_\rho(s) \tag{12g}$$

7.3 The torsional motion

In order to solve Eq. (9c), we are searching for a solution of the form

$$\varphi(x,t) = \sum_{\rho=1}^n \Phi_\rho(x)\cdot Z_\rho(t) \tag{13a}$$

where, $Z_\rho(t)$ are the time functions under determination and $\Phi_\rho(x)$ are functions arbitrarily chosen that satisfy the boundary conditions. As such functions we choose the shape functions for torsion of a single span beam, given by the following equations

$$\left.\begin{aligned} &\Phi_\rho(x) = c_1\left(\sin k_1 x - \frac{\sin k_1 L}{\mathrm{Sinh} k_2 L}\cdot \mathrm{Sinh} k_2 x\right) \\ &\text{where:}\quad k_1 = \sqrt{-\frac{G I_d}{2E I_w} + \sqrt{\left(\frac{G I_d}{2E I_w}\right)^2 + \frac{I_{px}\omega_{\varphi\rho}^2}{E I_w}}} \\ &k_2 = \sqrt{\frac{G I_d}{2E I_w} + \sqrt{\left(\frac{G I_d}{2E I_w}\right)^2 + \frac{I_{px}\omega_{\varphi\rho}^2}{E I_w}}} \end{aligned}\right\} \tag{13b}$$

while $\omega_{\varphi\rho}$ are given by following the relation

$$\omega_{\varphi\rho} = \sqrt{\frac{\rho^4\pi^4 E I_w}{I_{px} L^4} + \frac{\rho^2\pi^2 G I_d}{I_{px} L^2}},\quad \rho = 1, 2, 3, ... \tag{13c}$$

Introducing (13a) into (9c) and following the procedure of §7.1 we conclude to the system

$$\ddot{Z}_\rho + \frac{c_\varphi}{m}\dot{Z}_\rho + \omega_{\varphi\rho}^2 Z_\rho = \frac{\int_0^\alpha m_x\Phi_\rho dx}{I_{px}\int_0^L \Phi_\rho^2 dx}\cdot f_x(t) - \frac{b^2 B_V\int_0^L \Phi_\rho dx}{I_{px}\int_0^L \Phi_\rho^2 dx}\cdot\int_0^L\sum_{\rho=1}^n \Phi_\rho Z_\rho dx \tag{14a}$$

In order to solve the above system Eq. (14a), we use the Laplace Transformation with initial conditions $Z_\rho(0) = \dot{Z}_\rho(0) = 0$. We set

$$\left.\begin{aligned} &LZ_\rho(t) = N_\rho(s),\quad Lf_x(t) = F_x(s) \\ &L\dot{Z}_\rho(t) = s\cdot N_\rho(s),\quad L\ddot{Z}_\rho(t) = s^2\cdot N_\rho(s) \end{aligned}\right\} \tag{14b}$$

Therefore, the system of Eq. (14a) becomes

$$\left.\begin{aligned} &\gamma_{\rho1}N_1 + \gamma_{\rho2}N_2 + \cdots + \gamma_{\rho k}N_k + \cdots + \gamma_{\rho\rho}N_\rho + \cdots + \gamma_{\rho n}N_n = \Delta_\rho \\ &\text{where:}\quad \gamma_{\rho k} = \frac{b^2 B_V\int_0^L \Phi_\rho dx\int_0^L \Phi_k dx}{I_{px}\int_0^L \Phi_\rho^2 dx} \\ &\gamma_{\rho\rho} = \frac{b^2 B_V\left(\int_0^L \Phi_\rho dx\right)^2}{I_{px}\int_0^L \Phi_\rho^2 dx} + (s^2 + \frac{c_\varphi}{I_{px}}\cdot s + \omega_{\varphi\rho}^2) \\ &\Delta_\rho = \frac{\int_0^\alpha m_x\Phi_\rho dx}{I_{px}\int_0^L \Phi_\rho^2 dx}\cdot F_x(s) \end{aligned}\right\} \tag{15a}$$

and finally

$$Z_\rho(t) = L^{-1}N_\rho(s) \tag{15b}$$

8. The general case (coupled motion)

In this case it is $z_M \neq 0$ and therefore, Eqs. (8) are valid. From Eq. (8a), we observe that the vertical motion is independent and therefore the equations of §7.1 are valid. In order for the solution of the problem of coupled lateral-torsional motion to apply the Lagrange's equations, we consider the potential energy of the system.

We call K the kinetic energy, D the dynamic one, F the dissipation energy and Ω the work of the external forces.

8.1 The potential energy of the system

8.1.1 The kinetic energy

The kinetic energy is produced by the lateral-torsional motion of the deck and it is given by the following expression

$$K = \frac{m}{2}\int_0^L \left(\frac{\partial \upsilon}{\partial t}\right)^2 dx + \frac{I_{px}}{2}\int_0^L \left(\frac{\partial \varphi}{\partial t}\right)^2 dx \tag{16a}$$

8.1.2 The dynamic energy

The dynamic energy is caused by the stresses of the deck and the moments produced by the hangers. Thus, from the deck we have

$$\left.\begin{aligned} D_1 = \frac{1}{2}\int_0^L \left(EI_z\upsilon'''' - EI_z z_M \varphi'''' - 2H_o\upsilon'' + B_H \int_0^L \upsilon dx \right)\cdot \upsilon dx + \\ + \int_0^L (EI_w\varphi'''' - EI_z z_M \upsilon'''' - GI_d\varphi'')\cdot \varphi dx \end{aligned}\right\} \tag{16b}$$

while from the moments of the hangers we get

$$m_T = -b^2B_V \int_0^L \varphi dx + \alpha(z_M + \alpha)B_H \int_0^L \upsilon dx \qquad \text{and}$$

$$D_2 = \frac{1}{2}\int_0^L m_T \varphi dx = \frac{1}{2}\int_0^L \left(-b^2B_V\int_0^L \varphi dx + (z_M + \alpha)B_H \int_0^L \upsilon dx \right)\cdot \varphi dx \tag{16c}$$

Therefore, the total dynamic energy will be

$$D = D_1 + D_2 \tag{16d}$$

8.1.3 The dissipation energy

The dissipation energy of the system will be

$$F = \frac{1}{2}\int_0^L c_z \dot{\upsilon}^2 dx + \frac{1}{2}\int_0^L c_\varphi \dot{\varphi}^2 dx \tag{16e}$$

8.1.4 The work of the external forces

Finally, the work produced by the external forces is

$$\Omega = \int_0^L (p_y \cdot \upsilon + m_x \cdot \varphi - c_z\dot{\upsilon}_o\upsilon - m\ddot{\upsilon}_o\upsilon)dx \tag{16f}$$

8.2 The solution of the equations of the problem

We are searching for a solution of the form

$$\left.\begin{aligned} \upsilon(x,t) &= \sum_n V_n(x)R_n(t) \\ \varphi(x,t) &= \sum_n \Phi_n(x)R_n(t) \end{aligned}\right\} \tag{17}$$

where $R_n(t)$ are the time functions under determination and $V_n(x)$, $\Phi_n(x)$ are functions arbitrarily chosen that satisfy the boundary conditions. As such functions we choose the shape functions given by (12b) and (13b) respectively.

8.2.1 The kinetic energy

Introducing expressions (17) into eq (16a) we have

$$K = \frac{m}{2}\int_0^L \left(\sum_n V_n\dot{R}_n\right)^2 dx + \frac{I_{px}}{2}\int_0^L \left(\sum_n \Phi_n\dot{R}_n\right)^2 dx =$$

$$= \frac{m}{2}\int_0^L \sum_n V_n^2\dot{R}_n^2 dx + \frac{m}{2}\int_0^L \sum_n\sum_k 2V_nV_kR_nR_k dx$$

$$+ \frac{I_{px}}{2}\int_0^L \sum_n \Phi_n^2\dot{R}_n^2 dx + \frac{I_{px}}{2}\int_0^L \sum_n\sum_k 2\Phi_n\Phi_kR_nR_k dx$$

From the above equation, we obtain successively

$$\frac{\partial K}{\partial \dot{R}_\rho} = m\int_0^L \sum_{k=1}^n V_kV_\rho\dot{R}_k dx + I_{px}\int_0^L \sum_{k=1}^n \Phi_k\Phi_\rho\dot{R}_k dx .$$

After differentiation and taking into account the orthogonality conditions of V_ρ and Φ_ρ we obtain

$$\frac{d}{dt}\left(\frac{\partial K}{\partial \dot{R}_\rho}\right) = \ddot{R}_\rho \int_0^L (mV_\rho^2 + I_{px}\Phi_\rho^2)dx \tag{18a}$$

In addition

$$\frac{\partial K}{\partial R_\rho} = 0 \tag{18b}$$

8.2.2 The dynamic energy

Introducing (17) into (16d) and taking into account the orthogonality conditions we get

$$D = \frac{1}{2}\int_0^L \begin{pmatrix} EI_z\sum_n V_n''''R_n - EI_z z_M\sum_n \Phi_n''''R_n \\ -2H_o\sum_n V_n''R_n + B_H\int_0^L\sum_n V_nR_n dx \end{pmatrix}\cdot \sum_n V_nR_n dx$$

$$+ \frac{1}{2}\int_0^L \begin{pmatrix} EI_w\sum_n \Phi_n''''R_n - EI_z z_M\sum_n V_n''''R_n \\ -GI_d\sum_n \Phi_n''R_n \end{pmatrix}\cdot \sum_n \Phi_nR_n dx$$

$$+ \frac{1}{2}\int_0^L \begin{pmatrix} -b^2B_V\int_0^L\sum_n \Phi_nR_n dx \\ +\alpha(z_M+\alpha)B_H\int_0^L\sum_n V_nR_n dx \end{pmatrix}\cdot \int_0^L\sum_n \Phi_nR_n dx$$

From the above equation we get

$$\left.\begin{aligned} \frac{\partial D}{\partial R_\rho} = {} & EI_zR_\rho\int_0^L V_\rho''^2 dx - EI_z z_M\sum_{k=1}^n\left\{R_k\int_0^L(\Phi_\rho''V_k'' + \Phi_k''V_\rho'')dx\right\} \\ & + 2H_o\int_0^L\left(V_\rho'\sum_n V_n'R_n\right)dx \\ & + B_H\int_0^L V_\rho dx\int_0^L\sum_n V_nR_n dx + EI_wR_\rho\int_0^L \Phi_\rho''^2 dx \\ & + GI_d\int_0^L\left(\Phi_\rho'\sum_n \Phi_n'R_n\right)dx \\ & - b^2B_V\int_0^L \Phi_\rho dx\int_0^L\sum_n \Phi_n'R_n dx \\ & + \frac{(z_M+\alpha)}{2}B_H\left(\int_0^L V_\rho dx\int_0^L\sum_n \Phi_nR_n dx + \int_0^L \Phi_\rho dx\int_0^L\sum_n V_nR_n dx\right) \end{aligned}\right\} \tag{18c}$$

8.2.3 The dissipation energy

Introducing Eq. (17a) into Eq. (16e) we obtain

$$F = \frac{1}{2} c_z \int_0^L \left(\sum_n V_n \dot{R}_n \right)^2 dx + \frac{1}{2} c_\varphi \int_0^L \left(\sum_n \Phi_n \dot{R}_n \right)^2 dx$$

which concludes to the following relation

$$\frac{\partial F}{\partial \dot{R}_\rho} = \dot{R}_\rho \left(c_z \int_0^L V_\rho^2 dx + c_\varphi \int_0^L \Phi_\rho^2 dx \right) \tag{18d}$$

8.2.4 The work of the external forces

Introducing Eq. (17a) into Eq. (16f) we obtain

$$\Omega = \int_0^L p_y(x) f_y(t) \cdot \sum_n V_n R_n dx + \int_0^L m_x(x) f_x(t) \cdot \sum_n \Phi_n R_n dx - [c_y \dot{\upsilon}_o(t) + m \ddot{\upsilon}_o(t)] \int_0^L \sum_n V_n R_n dx$$

From the above we obtain

$$\left. \begin{aligned} \frac{\partial \Omega}{\partial R_\rho} &= f_y(t) \int_0^L p_y(x) V_\rho dx + f_x(t) \int_0^L m_x(x) \Phi_\rho dx \\ &- [c_y \dot{\upsilon}_o(t) + m \ddot{\upsilon}_o(t)] \int_0^L V_\rho dx \end{aligned} \right\} \tag{18e}$$

8.2.5 The Lagrange's equations

Applying the Lagrange's equations

$$\left. \begin{aligned} &\frac{d}{dt}\left(\frac{\partial K}{\partial \dot{R}_\rho} \right) - \frac{\partial K}{\partial R_\rho} + \frac{\partial D}{\partial R_\rho} + \frac{\partial F}{\partial \dot{R}_\rho} = \frac{\partial \Omega}{\partial R_\rho} \\ &\text{for} \quad \rho = 1 \text{ to } n \end{aligned} \right\} \tag{19a}$$

and taking into account Eq. (18a) to (18e) we obtain

$$\left. \begin{aligned} &\ddot{R}_\rho \int_0^L (m V_\rho^2 + I_{px} \Phi_\rho^2) dx + \dot{R}_\rho \int_0^L (c_z V_\rho^2 + c_\varphi \Phi_\rho^2) dx \\ &+ R_\rho \int_0^L (EI_z V_\rho''^2 + EI_w \Phi_\rho''^2) dx \\ &- EI_z z_M \sum_{k=1}^n \left\{ R_k \int_0^L (\Phi_\rho'' V_k'' + \Phi_k'' V_\rho'') dx \right\} + 2H_o \int_0^L V_\rho' \sum_n V_n' R_n dx \\ &+ GI_d \int_0^L \Phi_\rho' \sum_n \Phi_n' R_n dx + B_H \int_0^L V_\rho dx \int_0^L \sum_n V_n R_n dx \\ &- b^2 B_V \int_0^L \Phi_\rho dx \int_0^L \sum_n \Phi_n R_n dx + \\ &+ \frac{\alpha(z_M + \alpha)}{2} B_H \left(\int_0^L V_\rho dx \int_0^L \sum_n \Phi_n R_n dx + \int_0^L \Phi_\rho dx \int_0^L \sum_n V_n' R_n dx \right) = \\ &= f_y(t) \int_0^L p_y V_\rho dx + f_x(t) \int_0^L m_x \Phi_\rho dx \\ &- c_z \dot{\upsilon}_o(t) \int_0^L V_\rho dx - m \ddot{\upsilon}_o(t) \int_0^L V_\rho dx \\ &\text{with:} \quad \rho = 1 \quad \text{to} \quad n \end{aligned} \right\} \tag{19b}$$

In order to solve the above differential system (19b) we use the Laplace Transformation setting

$$\left. \begin{aligned} LR_\rho(t) &= G_\rho(s) \\ Lf_x(t) &= u_x(s) \\ Lf_y(t) &= u_y(s) \\ L\upsilon_o(t) &= U_o(s) \end{aligned} \right\} \tag{20a}$$

From the above and with initial conditions $R_\rho(0) = \dot{R}_\rho(0) = 0$ we obtain

$$\left. \begin{aligned} L\dot{R}_\rho(t) &= s \cdot G_\rho(s) \\ L\ddot{R}_\rho(t) &= s^2 \cdot G_\rho(s) \\ L\dot{\upsilon}_o(t) &= s \cdot U_o(s) \\ L\ddot{\upsilon}_o(t) &= s^2 \cdot U_o(s) \end{aligned} \right\} \tag{20b}$$

Therefore, the system of Eq. (19b) becomes

$$\left. \begin{aligned} &A_{\rho 1} G_1 + A_{\rho 2} G_2 + \ldots\ldots\ldots + A_{\rho\rho} G_\rho + .\rho\ldots\ldots\ldots + A_{\rho n} G_n = \Xi_\rho \\ &\text{with} \quad \rho = 1 \text{ to } n \quad \text{and:} \\ &A_{\rho k} = -EI_z z_M \int_0^L (\Phi_\rho'' V_k'' + \Phi_k'' V_\rho'') dx + 2H_o \int_0^L V_\rho' V_k' dx \\ &+ GI_d \int_0^L \Phi_\rho' \Phi_k' dx + B_H \int_0^L V_\rho dx \int_0^L V_k dx - b^2 B_V \int_0^L \Phi_\rho dx \int_0^L \Phi_k dx \\ &+ \frac{\alpha(z_M + \alpha)}{2} B_H \left(\int_0^L V_\rho dx \int_0^L \Phi_k dx + \int_0^L \Phi_\rho dx \int_0^L V_k dx \right) \\ &A_{\rho\rho} = s^2 \cdot \int_0^L (m V_\rho^2 + I_{px} \Phi_\rho^2) dx + s \cdot \int_0^L (c_z V_\rho^2 + c_\varphi \Phi_\rho^2) dx \\ &+ \int_0^L (EI_z V_\rho''^2 + EI_w \Phi_\rho''^2) dx - 2EI_z z_M \int_0^L \Phi_\rho'' V_\rho'' dx \\ &+ 2H_o \int_0^L V_\rho'^2 dx + GI_d \int_0^L \Phi_\rho'^2 dx + B_H \left(\int_0^L V_\rho dx \right)^2 - b^2 B_V \left(\int_0^L \Phi_\rho dx \right)^2 \\ &+ \alpha(z_M + \alpha) B_H \int_0^L V_\rho dx \int_0^L \Phi_\rho dx \\ &\Xi_\rho = u_y(s) \int_0^L p_y V_\rho dx + u_x(s) \int_0^L m_x \Phi_\rho dx - c_y s U_o(s) \int_0^L V_\rho dx - ms^2 U_o(s) \int_0^L V_\rho dx \end{aligned} \right\} \tag{20c}$$

Solving the above system, we get the functions $G_\rho(s)$ and, therefore

$$R_\rho(t) = L^{-1} G_\rho(s) \tag{20d}$$

9. Numerical results and discussion

Let us consider a simply supported footbridge with span length L=40 m and width b=3 m. The bridge is made from structural steel (isotropic and homogeneous material) with modulus of elasticity $E = 2.1 \times 10^8 kN/m^2$, shear modulus $G = 0.8 \times 10^8 kN/m^2$, moments of inertia $I_y = 0.001\ m^4$, $I_z = 0.030\ m^4$, $I_d = 0.0005\ m^4$, warping constant $I_w = 0.100 m^6$, mass per unit length m=200 kg/m, damping coefficient β=0.05 and rotational mass inertia $I_{px} = 1000\ kgm^2$.

A cable system such as the one shown in Fig. 2 is applied on this bridge, with the following characteristics: $E_c = 9 \cdot 10^8 kN/m^2$, cable's diameter d=4 cm or cable's cross-section required $F_c = 12 \cdot 10^{-4} m^2$ (by considering a allowed tension $5000\ dN/cm^2$), different f_o, varying from 5 to 15m. Particularly the values $f_o = 5, 10, \text{and } 15m$ will be study, which correspond to $H_o = 60000, 30000, \text{and } 20000\ dN$, respectively.

In order to evaluate the cables' influence under the most unfavorable loading cases on the bridge's behavior, we will study firstly the bridge without cables.

9.1 Bridge without cables

The equations for free and forced motion corresponding to this case are given in the Appendix.

In this section, the behavior of a pedestrian bridge under

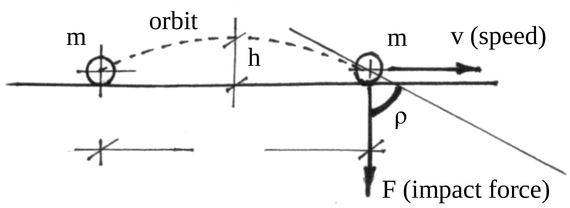

Fig. 6 The impact phenomenon

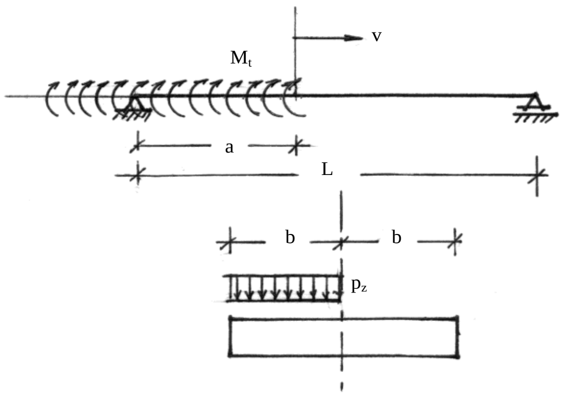

Fig. 7 The loading of a military force

Table 1 Characteristics of human crowd loading

v (m/sec)	0.5	1.0	1.4	1.5	2.0	2.5	3.0	3.5	4.0	5.0	6.0
T (sec)	1.10	1.00		0.90		0.70		0.50		0.35	0.30
kind of walk	walking			Light jogging		jogging				running	
Stride	$\ell=0.75$ $h=0.07$ ρ=1.213			$\ell=1.10$ h = 0.15 ρ=1.071		$\ell=1.50$ $h=0.25$ ρ=0.983					
Equation	$p_z=\frac{p_o}{2}\cdot\left[1+(1+\varepsilon)\cdot\frac{v\cdot\cos\alpha}{g}\right]\cdot\left[1+\cos\left(\frac{2\pi}{T}\cdot t\right)\right]$									------	

Table 2 Maximum and minimum deflection w for various load speeds

v (m/sec)	0.5	1.0	1.5	2.0	2.5	3.0	3.5	4.0
max w (m)	0.177	0.178	0.195	0.205	0.210	0.221	0.224	0.238
min w (m)	0.115	0.129	0.153	0.167	0.190	0.203	0.212	0.225
amplitude (m)	0.062	0.049	0.042	0.038	0.020	0.018	0.012	0.013

the action of human crowd and seismic loadings is studied in order to identify the most unfavorable intervals of frequency and speed of a human crowd loading.

Although the human crowd load depends on many random factors, i.e., Musse and Thalmann (1997), Lee and Hughes (2006), there is a load that is the most dangerous one and, simultaneously, can be expressed by a simple mathematical formula, Akopov and Beklaryan (2012) and Dagbe (2012). This is the case of a military force marching with rhythmic step that produces vertical, lateral and torsional vibrations. The military force can be walking or jogging with some speed v with the characteristics given in Table 1.

The walkers, the joggers or the runners have not a

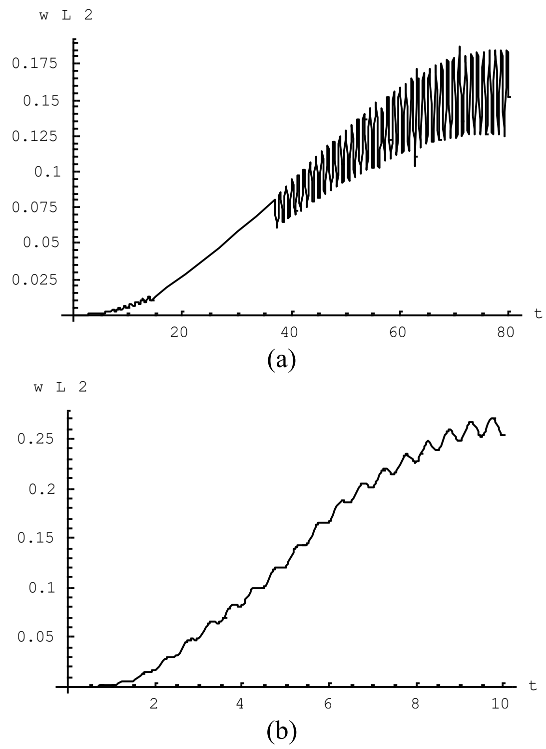

Fig. 8 Deflections at the middle of the bridge for (a) v=0.5and (b) v=4 m/sec

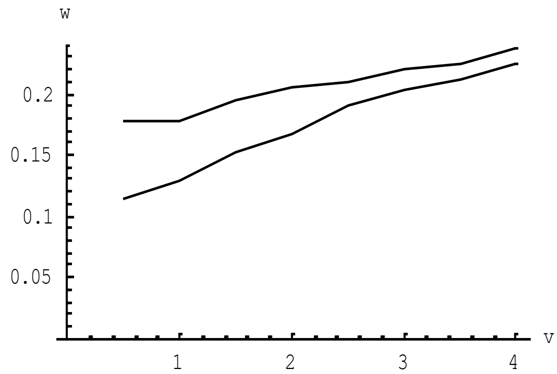

Fig. 9 Maximum and minimum deflections at the middle of the bridge

Table 3 Maximum and minimum angles of rotation

v (m/sec)	0.5	1.0	1,5	2.0	2,5	3.0	3.5	4.0
max φ (m)	0.45	0.26	0.18	0.06	0.025	0.025	0.018	0.017
min φ (m)	-0.40	-0.24	-0.10	-0.08	-0.035	-0.033	-0.020	-0.018
Amplitude (rad/deg°)	0.85 48.7°	0.50 28.6°	0.28 16.0°	0.14 5.1°	0.060 3.4°	0.058 3.3°	0.038 2.2°	0.035 2°

continuous contact with the deck. This kind of loading can be approximated by the equation

$$p_o(x,t)=p_o(x)\cdot\frac{1}{2}\cdot\left[1+\cos\left(\frac{2\pi}{T}\cdot t\right)\right],$$ where T is the contact period of the marching military force depending, according to the Table 1, on the speed v as given by Wollzenmuller (2010). On the other hand, one must evaluate and take into account the impact phenomenon

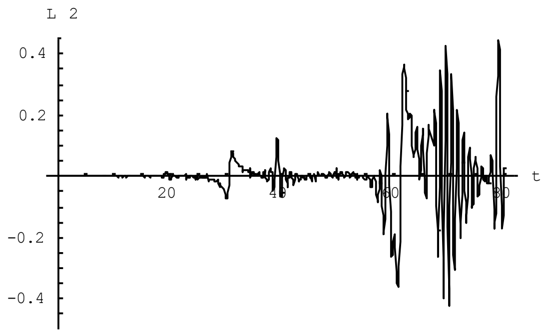

(a)

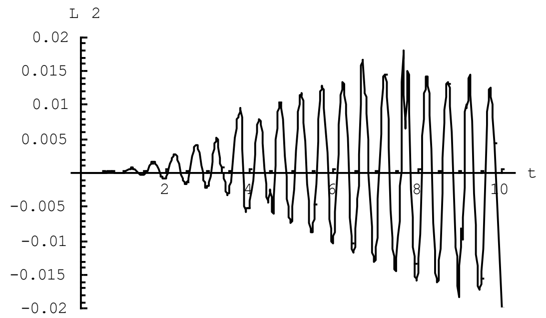

(b)

Fig. 10 Rotation angles at the middle of the bridge for (a) v=0.5 and (b) v=4 m/sec

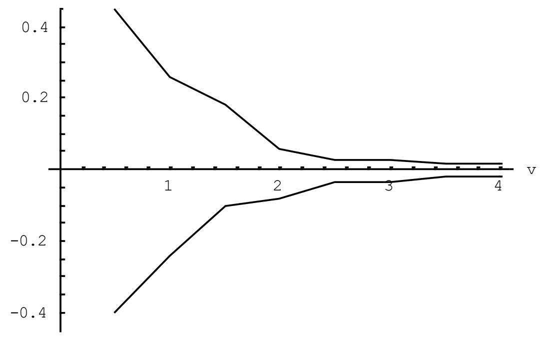

Fig. 11 Maximum and minimum rotation angles at the middle of the bridge

appearing when someone runs. This causes an increase of the loading, depending on the speed, on the stride of the runners and mainly on the coefficient of restitution. This last varies from 0.88 to 0.92 as shown by Elert (2006). Thus, the acting load can be written as: $p_z = p_o(x,t) + (1+\varepsilon)\cdot m\cdot v\cdot\cos\alpha$, where α is shown in Fig. 6, and m the mass of the runner. Therefore, the finally acting loading will be

$$p_z = \frac{p_o}{2}\cdot\left[1+(1+\varepsilon)\cdot\frac{v\cdot\cos\rho}{g}\right]\cdot\left[1+\cos\left(\frac{2\pi}{T}\cdot t\right)\right] \tag{21}$$

We will limit our research up to speed value of 4 m/sec.

The final loading, except of the vertical motion, produces also a torsional one, caused by the torsional moment M_t which depends on the eccentricity of the distributed load p_z. The worst loading case is shown in Fig.

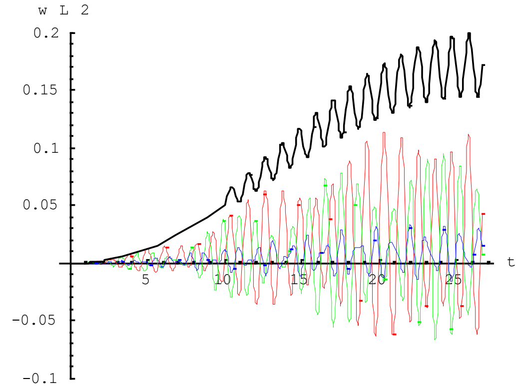

Fig. 12 Influence of angle θ for f_o=5 m. without cables (black), θ=10° (red), θ=15° (green), θ=20° (blue)

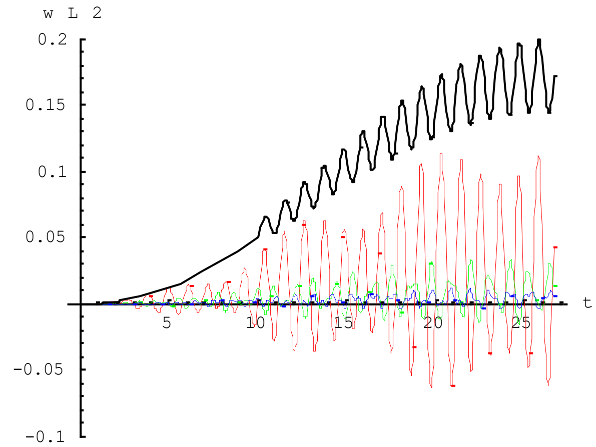

Fig. 13 Influence of sag f_o for θ=10°.without cables (black), f_o=5 m (red), f_o=10 m (green), f_o=15 m (blue)

6, where the distributed load is moved on the left half of the deck. The studied cases are shown in Fig. 7.

9.1.1 The vertical motion

Applying the formulae given in the Appendix for a range of speeds from 0.5 to 4 m/sec, we obtain the Table 2, where the maximum and minimum deflections w are shown.

In the diagram of Fig. 8 one can see the deflections of the middle of the bridge for speed v=0.5 m/sec (Fig. 8(a)) and v=4 m/sec (Fig. 8(b)).

From the above results we ascertain that for the studied range of speeds the deflections of the middle of the bridge differ slightly, while the deflections' amplitude is greater as the speed is lower (see and diagram of Fig. 9).

9.1.2 The torsional motion

Applying the formulae given in the Appendix for a range of speeds from 0.5 to 4 m/sec, we obtain the Table 3, where the maximum and minimum angles φ are shown.

In the diagram of Fig. 10 are shown the rotation angles of the middle of the bridge for speed v=0.5 m/sec (Fig. 10(a)) and v=4 m/sec (Fig. 10(b)).

From the above results we ascertain that for the studied range of speeds the rotation angles of the middle of the

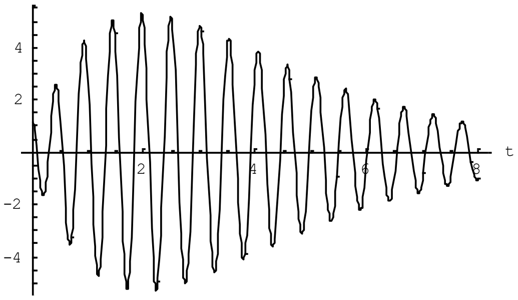

Fig. 14 Accelerogram of the ground motion

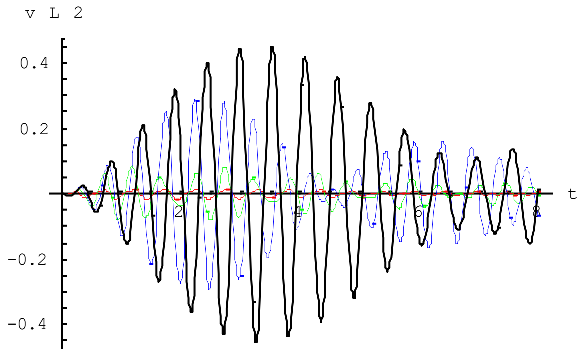

Fig. 15 Influence of angle θ for f_o=5 m without cables (black), θ=10° (red), θ=60° (green), θ=70° (blue)

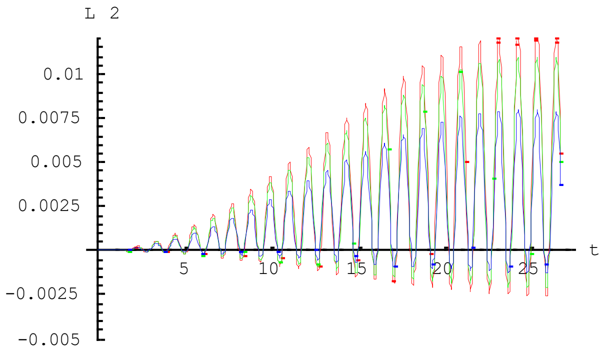

Fig. 16 Influence of angle θ for f_o=5 m. θ=10° (red), θ=20° (green), θ=40° (blue)

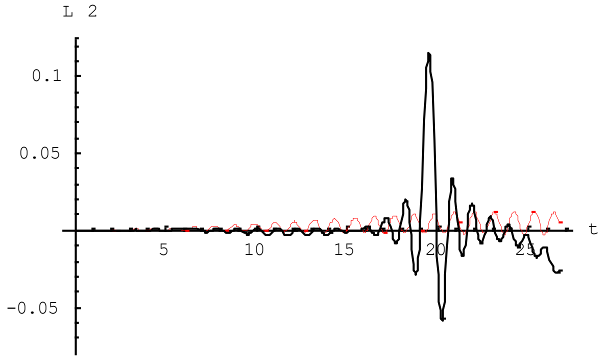

Fig. 17 Rotation angles of the middle of the bridge for f_o=5 m. without cables (black), and θ=10° (red)

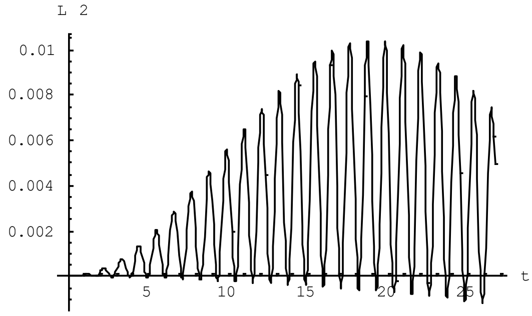

(a)

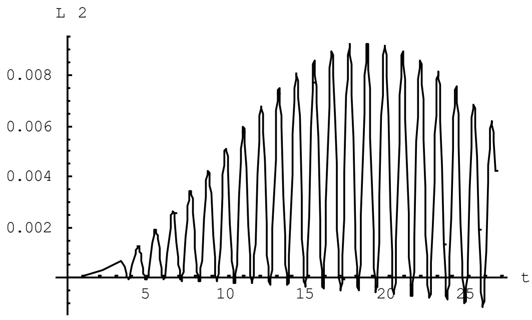

(b)

Fig. 18 Influence of z_M and α for θ=10° and f_o=5. z_M=0.5 m, α=0 and (b) z_M=1.0 m, α=2.0 m

bridge depend considerably on the speed v, while the rotation angles' amplitude is greater as the speed is lower (see and diagram of Fig. 11).

9.2 Bridge with cross-section of double symmetry

Studying the behavior of a bridge without cables, we conclude to the plots of Fig. 9 (for vertical motion) and of Fig. 11 (for torsional motion).

We select to study the lateral motion for $\upsilon = 1.5\,\text{m/sec},\ T = 1.10\,\text{sec}$, and the torsional one for $\upsilon = 1.0\,\text{m/sec},\ T = 1.00\,\text{sec}$.

9.2.1 The vertical motion

Applying the equations of §7.1 we will study the influence of angle θ and of sag f_o. Studying the influence of angle θ (Fig. 2) of the cables for f_o=5 m, we obtain the plots of Fig. 12. We observe that even for small values of the angle θ the decrease of the deformations is considerable.

Particularly, for θ = 10°, the decrease amounts to ~40%, for θ = 15°, the decrease amounts to ~55%, while for θ = 20°, the decrease amounts to ~75%.

For θ = 10°, we are studying the influence of f_o (Fig. 2) gathering the plots of Fig. 13. We see that the influence of the sag f_o is also considerable.

Particularly, for f_o = 5 m, the decrease amounts to ~40%, for f_o = 10 m the decrease amounts to ~75%, while for f_o = 15 m the decrease amounts to ~90%.

9.2.2 The lateral motion

It is assumed that the above bridge is subjected to an earthquake action, where the ground motion is given by: $\upsilon_o = \alpha \cdot t \cdot e^{-k \cdot t} \cdot \sin\Omega t$, with $\alpha = 0.05,\ k = 0.50,\ \Omega = 12\,\text{sec}^{-1}$,

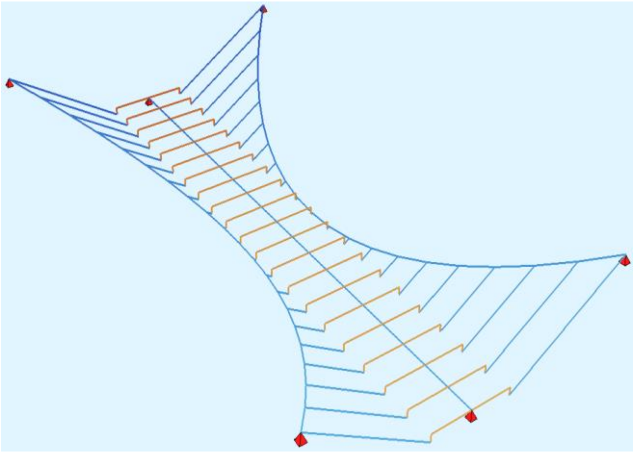

Fig. 19 Finite element model of the bridge with L=40 m, θ=20°, f_o=10 m and z_m=0.5 m

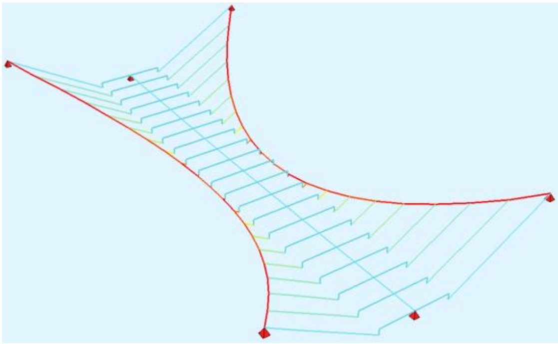

(a)

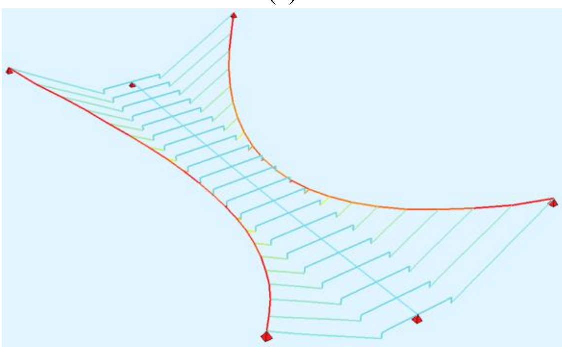

(b)

Fig. 20 Stress and deformed states due to (a) concentric load and (b) eccentric load with e=1.5 m

which gives the accelerogram shown in Fig. 14.

In order to study the influence of the cables' system on the bridge's behavior, we apply the equations of §7.2, considering three cases:

a) f_o = 5 m and θ = 10°, b) f_o = 5 m and θ = 60° and c) f_o = 5 m and θ = 70°.

We find out that for small values of θ the effect is very strong (decrease of deformations ~95%), while for values greater than θ = ~65°, this effect decreases dramatically (for θ = 60° the decrease is ~65% and for θ = 70° the decrease is ~45%).

9.2.3 The torsional motion

We assume next that the above bridge is subjected to an eccentric loading due to human crowd moving with a velocity v. This eccentricity produces a torsional moment $M_t(x,t)$, (see Fig. 5). Therefore, the term of equation (14a) containing the torsional moment becomes

$$\int_0^L M_t(x,t)\Phi_\rho(x)dx = \int_0^\alpha M_t(x,t)\Phi_\rho(x)dx = \int_0^{\upsilon\cdot t} M_t(x,t)\Phi_\rho(x)dx$$

$$M_t = \frac{p_z b^2}{2} \text{ and } p_z = \frac{p_o}{2}\cdot\left[1+(1+\varepsilon)\cdot\frac{v\cdot\cos\alpha}{g}\right]\cdot\left[1+\cos\left(\frac{2\pi}{T}\cdot t\right)\right]$$

$$,\quad p_o = 200\,\mathrm{dN/m^2}$$

9.3 Bridge with cross-section of one axis of symmetry (the general case)

In the previous sections it has been assumed that z_M=α=0 for various values of f_o and θ. In this section we proceed to estimate the influence of the distance z_M between the shear and gravity centers and of the distance α between the hangers' anchorage point and the gravity center on the effectiveness of an external cable system. For this purpose, we are employing a standard cable system with:

θ=10° and f_o=5 m and we study the influence of the last term of Eqs. (7) or (8c) which includes the summation (z_M+α).

Applying the equations of §7.3 we obtain the plots of Figs. 16 and 17.

From the plots of Fig. 17, we see that the effect of the cable system is remarkable and the decrease of the rotation angle amounts to ~90%, while from the plots of Fig. 16, we see that for angles θ>10° the decrease of the angle φ is significantly greater.

Fig. 18(a), with z_M=0.5 m and α=0 gives φ_{max}=0.0112 m, which differs slightly from the red diagram of Fig. 16 (where z_M=α=0) and gives φ_{max}=0.0115 m (difference ~3%). Applying next the extreme values z_M=1.0 m and α=2.0 m (which are almost non-realistic for a footbridge with the studied length), we obtain the plot of Fig. 18(b) that gives φ_{max}=0.0097 m which compared to the one of Fig. 18(a) with φ_{max}= 0.0112 m shows that the influence of the summation (z_M+α) on the effectiveness of the applied external cables system results in a decrease of about 13% of the φ_{max}.

Comparing both results φ_{max} from Fig. 18 with the one from Fig. 17, we see that the system of external cables with z_M=α=0 provides a decreasing of the maximum value of φ of about 90%. From the above results we ascertain that the term z_M slightly affects the rotation angles of the bridge, while for bigger values of z_M and α (approaching non-realistic values) we see that this influence increases but in not remarkable levels.

10. Finite elements analyses

In order to validate the analytical models presented herein, a number of numerical analyses via the finite element method have been performed. For this purpose, the FEM analysis software by SOFISTIK has been employed and the above bridge has been modeled regarding the bridge

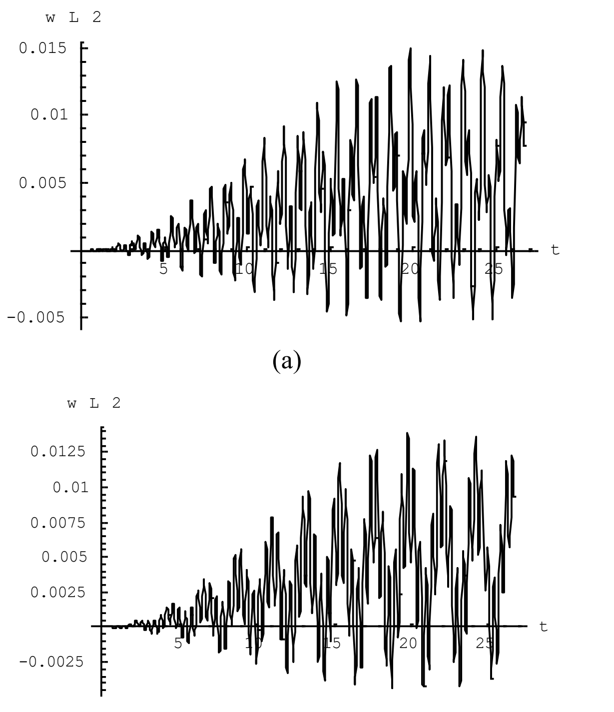

Fig. 21 Vertical deflection due to concentric load: (a) analytical model and (b) finite element model

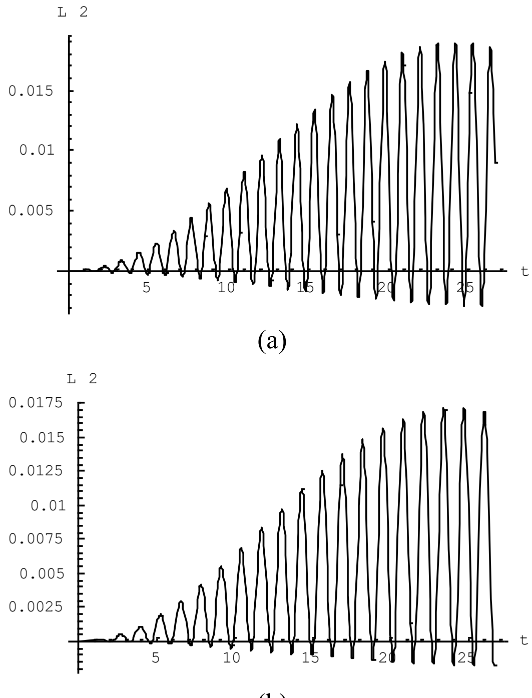

Fig. 22 Rotation angle due to eccentric load: (a) analytical model and (b) finite element model

deck and the cables with the same material and cross-sectional properties as in Section 9. Only the case with θ=20°, f_o=10 m, z_m=0.5 m and live load p=500 dN/m^2 moving with constant velocity v=1.5m/s is considered. Both cases of concentric and eccentric load with e=1.5 m have been investigated.

The bridge deck has been modeled with 160 beam elements along the longitudinal axis, while in the transverse direction the hangers are connected to the deck-beam with rigid link elements. A dense arrangement of hangers every 2.0 m along the length of the bridge has been considered in the model. Both cables and hangers have been modeled with cable elements (see Fig. 19).

The bridge models have been analyzed via non-linear time-history analyses, where the loading history has been manually introduced to the nodes of the deck-beam in the form of vertical forces (for concentric load) and vertical forces and moments (for eccentric load).

In Fig. 20, one can schematically see the stress and deformed states of the bride at time t=25 s just before the load reaches the end of the bridge. The model in

Fig. 20(a) corresponds to concentric load passage, while in Fig. 20(b) to eccentric load passage.

In Fig. 21 one can see the vertical response of the bridge at the mid-length obtained for concentric load passage: (a) via the analytical model presented herein and (b) via the finite element model. From the response diagrams of Fig. 21 it has been found that the maximum amplitude of w from the FE analysis is 0.01455 m (Fig. 21(b)), while the maximum amplitude from the analytical model is 0.01510 m (Fig. 21(a)). Hence, there is a 3.8% difference between the maximum amplitudes from the two analyses.

In Fig. 22, one can see the rotation angle responses of the bridge at the mid-length due to eccentric load passage. The maximum values of the amplitudes of φ are 0.0187 rad from the FE analysis (Fig. 22(b)) and 0.0173 rad from the analytical model (Fig. 22(a)), respectively, and the difference is almost 6.2%.

The same pattern for both numerical models is observed also for the beam and cable forces and stresses. From the above analyses, it can be concluded that the finite element models are slightly stiffer than the analytical ones and can also predict the dynamical response of the bridge with sufficient accuracy.

11. Conclusions

From the above bridge model and the results presented herein, one can draw the following conclusions:

• A mathematical model for the study of bridges strengthened by external cable system for the study of its dynamic behavior is proposed.

• A system of external cables can act as a very efficient damping system, which can be applied in existing bridges (especially pedestrian ones) that are facing dynamic problems after their erection (probably due to bad design). The exposed results:

• are the most unfavorable for the reason that the applied loads are extremely unfavorable.

• The walking velocities v are critical for values v<1.5 m/sec, while for very low walking speeds (v<0.3 m/sec) the torsional deformations φ become maximum.

• The possible applied cable system is efficient for reduction of the vertical, lateral, and also the torsional motion.

• For the vertical motion, the decrease of the deformations amounts for about 40 to 75% for relatively small angles θ while it becomes even more efficient if combined with a proper selection of sag f_o.

• For the lateral motion, as it was expected, the cable system is remarkably effective where the lateral deformations decrease up to 95%. Even for big values of θ, one has a satisfactory reduction of the lateral motion amplitudes.

• For the dynamic torsional motion, one can see that the effect of the cable system is remarkable and the decrease of the rotation angle amounts up to ~90%, while for angles $\theta > 10^o$ the decrease of the torsional angle φ is significantly greater.

• The influence of z_M is not considerable and its presence slightly affects the rotation angles of the bridge. For bigger values of z_M and α (approaching non-realistic values) one can see an enhanced influence but in not remarkable levels.

• The analytical method presented herein has been verified via the finite element method with sufficient accuracy.

• Finally, one can ascertain that a detailed design should take into account all combinations of the above factors involved in the preceding analysis.

References

Akopov, A.S. and Beklaryan, L.A. (2012), "Simulation of human crowd behavior in extreme situations", *Int. J. Pure Appl. Math.*, **79**(1), 121-138.

Bachmann, H. and Ammann, W. (1987), *Vibrations in Structures-Induced by Man and Machines*, Structural Engineering Document, No.3e, IABSE, Zurich, Switzerland.

Dagbe, C. (2012), "On the modeling of crowd dynamics by generalized kinetic models", *J. Math. Analy. Appl.*, **385**(2), 512-532.

Dallard, P., Fitzpatrick, A.J., Flint, A. and Ridsdill Smith, R.M. (2001), "The London millennium footbridge", *Struct. Eng.*, **79**(22), 17-33.

Eckhard, B. and Ott, E. (2006), "Crowd synchrony on the London millennium bridge", *Chaos*, **16**(4), 041104.

Elert, G. (2006), *Experiments for Determine the c.o.r. for Impact of Various Balls on a Concrete Surface*, Edition of Midwood High School, Brooklyn, New York, U.S.A.

Fujino, Y., Pacheco, B., Nakamura, S. and Warnitcahi, P. (1993), "Synchronization of human walking observed during lateral vibration of a congested pedestrian bridge", *Earthq. Struct. Dyn.*, **22**(9), 741-758.

Fujino, Y., Sun, L., Pacheco, B. and Chaiseri, P. (1992), "Tuned Liquid Damper (TLD) for suppressing horizontal motion of structures, *J. Eng. Mech.*, **118**(10), 2017-2030.

Ingólfsson, E.T. and Georgakis, C.T. (2011), "A stochastic load model for pedestrian-induced lateral forces on footbridges", *Eng. Struct.*, **33**(12), 3454-3470.

Ingólfsson, E.T., Georgakis, C.T. and Jönsson, J. (2012), "Pedestrian-induced lateral vibrations of footbridges: A literature review", *Eng. Struct.*, **45**, 21-52.

Lee, R.S.C. and Hughes, R.L. (2006), "Prediction of human crowd pressures", *Accid. Analy. Prevent.*, **38**(4), 712-722.

Li, Z., Li, P., He, Z. and Cao, P. (2013), "Static and free vibration analysis of shallow sagging inclined cables", *Struct. Eng. Mech.*, **45**(2), 145-157.

Lonetti, P. and Pascuzzo, A. (2014), "Design analysis of the optimum configuration of self-anchored cable-stayed suspension bridges", *Struct. Eng. Mech.*, **51**(5), 847-866.

Michaltsos, G.T. and Raftoyiannis, I.G. (2012), *Bridges' Dynamics*, Bentham Sciences Publication, U.A.E.

Musse, S.R. and Thalmann, D. (1997), "A model of human crowd behavior: Group inter-relationship and collision detection analysis", *Computer Animation and Simulation*, *Proc. Eurographics Workshop*, Budapest, Hungary.

Nakamura, S. and Kawasaki, T. (2006), "Lateral vibration of footbridges by synchronous walking", *J. Constr. Steel Res.*, **62**(11), 1148-1160.

Racic, V. and Morin, J.B. (2014), "Data-driven modeling of vertical dynamic excitation of bridges induced by people running", *Mech. Syst. Sign. Proc.*, **43**(1-2), 153-170.

Roberts, G.W., Meng, X., Brown, C.J. and Dallard, P. (2006), "GPS measurements on the London millennium bridge", *Proceedings of the Institution of Civil Engineers: Bridge Engineering*, **159**(4), 153-161.

SOFiSTiK AG (2016), *Online User Manual*, <http://www.sofistik.eu>.

Stoyanoff, S.D. (1992), "A unified approach for 3D stability and time domain response analysis with application of quasi-steady theory", *J. Eng. Mech.*, **118**, 2017-2030.

Sun, B., Zhang, L., Qin, Y. and Xiao, R. (2016), "Economic performance of cable supported bridges", *Struct. Eng. Mech.*, **59**(4), 621-652.

Wollzenmuller, F. (2010), *Richtig Laufen Technik, Training, Laufprogramme*, 3rd Edition, BLV-Sport Praxis, Broschiert.

Zhang, X. and Yu, Z. (2015), "Study of seismic performance of cable-stayed-suspension hybrid bridges", *Struct. Eng. Mech.*, **55**(6), 1203-1221.

Zhang, X. and Zhang, C. (2016), "Study of seismic performance and structural system of suspension bridges", *Struct. Eng. Mech.*, **60**(4), 595-614.

CC

Appendix

a. The vertical or lateral motion

The equation of motion is the same for both the above cases

$$\left.\begin{aligned}&\text{Vertical motion: } EI_y w'''' + c\dot{w} + m\ddot{w} = p_y(x)\cdot f_y(t)\\&\text{Lateral motion: } EI_z \upsilon'''' + c\dot{\upsilon} + m\ddot{\upsilon} = p_z(x)\cdot f_z(t)\end{aligned}\right\} \quad (a.1)$$

Shape functions

$$\left.\begin{aligned}&\text{Vertical motion: } w_n(x) = \frac{n\pi x}{L}\\&\text{Lateral motion: } \upsilon_n(x) = \frac{n\pi x}{L}\end{aligned}\right\} \quad (a.2)$$

Eigenfrequencies

$$\left.\begin{aligned}&\text{Vertical motion: } \omega_{yn} = \sqrt{\frac{n^4\pi^4 E I_y}{m L^4}}\\&\text{Lateral motion: } \omega_{zn} = \sqrt{\frac{n^4\pi^4 E I_z}{m L^4}}\end{aligned}\right\} \quad (a.3)$$

Forced motion under the action of a distributed dynamic load

$$w(x,t) = \sum_n W_n(x)\cdot F_n(t) \quad (a.4)$$

with

$$\left.\begin{aligned}&F_n(t) = \frac{\int_0^L p_y(x)W_n(x)dx}{m\overline{\omega}_{yn}\int_0^L W_n^2(x)dx}\cdot\int_0^t f_y(\tau)\cdot e^{-b(t-\tau)}\sin\overline{\omega}_{yn}(t-\tau)d\tau,\\&\beta = \frac{c}{2m},\quad \overline{\omega}_{yn} = \sqrt{\omega_{yn}^2 - \beta^2}\end{aligned}\right\} \quad (a.5)$$

Forced motion under the action of a distributed moving load with speed υ

$$w(x,t) = \sum_n W_n(x)\cdot F_n(t) \quad (a.6)$$

with

$$\left.\begin{aligned}&F_n(t) = \frac{1}{m\overline{\omega}_{yn}\int_0^L W_n^2(x)dx}\cdot\int_0^t\left(\int_0^{\upsilon\cdot\tau} p_y(x)W_n(x)dx\right)f_y(\tau)\cdot e^{-b(t-\tau)}\sin\overline{\omega}_{yn}(t-\tau)d\tau\\&\beta = \frac{c}{2m},\quad \overline{\omega}_{yn} = \sqrt{\omega_{yn}^2 - \beta^2}\end{aligned}\right\} \quad (a.7)$$

b. The torsional motion

Equation of motion

$$EI_w\varphi'''' - GI_d\varphi'' + c\dot{\varphi} + I_{px}\ddot{\varphi} = m_x(x)\cdot f_x(t) \quad (b.1)$$

Eigenfrequencies

$$\omega_{\varphi n} = \sqrt{\frac{n^4\pi^4 EI_w}{I_{px}L^4} + \frac{n^2\pi^2 GI_d}{I_{px}L^2}} \quad (b.2)$$

Shape functions

$$\left.\begin{aligned}&\Phi_n(x) = \sin\lambda_1 x - \frac{\sin\lambda_1 L}{\mathrm{Sinh}\lambda_2 L}\cdot\mathrm{Sinh}\lambda_2 L\\&\text{with: } \lambda_1 = \sqrt{-\frac{GI_d}{2EI_w} + \sqrt{\left(\frac{GI_d}{2EI_w}\right)^2 + \frac{I_{px}\omega_{\varphi n}^2}{EI_w}}}\\&\lambda_2 = \sqrt{\frac{GI_d}{2EI_w} + \sqrt{\left(\frac{GI_d}{2EI_w}\right)^2 + \frac{I_{px}\omega_{\varphi n}^2}{EI_w}}}\end{aligned}\right\} \quad (b.3)$$

For the case of a distributed moving moment with speed υ

$$\varphi(x,t) = \sum_n \Phi_n(x)\cdot R_n(t) \quad (b.4)$$

with

$$\left.\begin{aligned}&R_n(t) = \frac{1}{I_{px}\overline{\omega}_{\varphi n}\int_0^L \Phi_n^2(x)dx}\cdot\int_0^t\left(\int_0^{\upsilon\cdot\tau} m_x(x)\Phi_n(x)dx\right)f_x(\tau)\cdot e^{-b(t-\tau)}\sin\overline{\omega}_{\varphi n}(t-\tau)d\tau\\&\beta = \frac{c}{2I_{px}},\quad \overline{\omega}_{\varphi n} = \sqrt{\omega_{\varphi n}^2 - \beta^2}\end{aligned}\right\} \quad (b.5)$$